Experimental Mechanics
https://doi.org/10.1007/s11340-024-01059-9

RESEARCH PAPER

Experimental Study of Nitinol Springs: Apparatus and Results

I. Alexandron[1] · **G. deBotton**[1,2]

Received: 18 April 2023 / Accepted: 19 March 2024

Abstract

Background The behavior of shape memory alloys that admit large reversible deformations in response to thermal excitation has been extensively studied in recent years. Yet, the number of works dealing with springs made from these alloys is rather limited in spite of their attractiveness in various applications.

Objective To bridge this gap we designed and constructed an experimental system for characterizing the behavior of the springs. It enables precise control of the three state variables: temperature, elongation, and force.

Methods Control of the sample temperature is achieved by immersing it in a water-filled thermal bath, where the water temperature is adjusted using a *thermoelectric Peltier* device. A tension-compression motorized unit sets the spring elongation and a force gauge is used for measuring the force exerted on the spring. The data is continuously monitored and acquired with a self-coded LabVIEW program. An important aspect is the calibration procedure developed for identifying the spring load-free state and ensuring the repetitiveness of the measurements.

Results Experiments in which the elongation or the force were measured as a function of the temperature demonstrate the role of the phase transformations. Isothermal experiments enabled to characterize the variations of the force versus the elongation at different temperatures.

Conclusions The proposed system facilitates the execution of highly accurate experiments through which the complex history-dependent behavior of shape memory springs can be revealed and studied.

Keywords Experimental system · Nitinol springs · Shape memory alloys · Calibration procedure

Introduction

Shape Memory Alloys (SMAs) exhibit two distinct characteristics. The first is the *Shape Memory Effect* (SME), which allows them to return to their original parent shape after undergoing significant and seemingly plastic deformation when heated. The second feature, referred to as *super-elasticity*, is the capability to isothermally experience substantial deformations and then revert to the original parent shape during a loading-unloading cycle [1]. SMAs have two crystalline phases: the *austenite* (A) high-temperature phase and the *martensite* (M) low-temperature phase [2]. When SMA in the austenite phase is cooled, it undergoes a *forward martensitic transformation* that starts at the *martensite start temperature* (M_s) and ends at the *martensite finish temperature* (M_f) [3, 4]. When no load is exerted during the process, the austenite transforms to a *twinned martensitic* state (M^t) while the original shape of the body is retained. When cooled under an external load, the material undergoes substantial deformation as the austenite transforms into *detwinned martensite* (M^d). Below the transformation temperature, this deformation remains unrecoverable even after the load is removed. When SMA in the martensitic state is heated, it transforms back to the austenite phase and the original shape of the body is recovered. This transformation, referred to as the *reverse martensitic transformation*, starts at the *austenite start temperature* (A_s) and ends at the *austenite finish temperature* (A_f) [3, 4].

The large forces associated with the reverse transformation of SMAs, alongside their high power-to-weight ratio, compared with other technologies, make the SMAs very attractive as thermally stimulated actuators. As an example, SMAs have a power-to-weight ratio typically 50 times greater than that of a DC motor, while being 100 times lighter in weight. When compared to a pneumatic motor,

✉ I. Alexandron
alexandi@post.bgu.ac.il

G. deBotton
debotton@bgu.ac.il

[1] Dept. of Biomedical Engineering, Ben-Gurion University of the Negev, Beer-Sheva 8410501, Israel

[2] Dept. of Mechanical Engineering, Ben-Gurion University of the Negev, Beer-Sheva 8410501, Israel

Published online: 10 May 2024

SMAs are 500 times lighter while maintaining a comparable power-to-weight ratio [5]. The most suitable SMA alloys for engineering applications are based on either Cu (mostly Cu-Zn-Al and Cu-Al-Ni) or NiTi [6, 7]. NiTi SMAs are more reliable, biocompatible, and have larger actuation stress and larger recoverable strain. Therefore, NiTi-based SMAs are the more natural choice in biomedical and microelectromechanical system applications [7–9], which is why they are being studied in the present research.

The elongation per length associated with the reverse transformation of SMA springs can reach several hundred percent, in contrast to just a few percent observed in SMA wires subjected to the same recoverable strain. This feature makes the springs more attractive as actuators [10–13]. Despite this advantage, the study of SMA springs has not progressed as extensively as that of SMA wires [14], and there is still a lack of an engineering model for them. Developing and building an experimental system to advance the study of shape memory springs is the first goal of this study.

The behavior of SMAs is governed by three state variables: temperature, strain, and stress, along with their rates and histories. The distinctive solid-solid phase transformation in SMAs means that even a minor deviation in one of the state variables, particularly temperature, can lead to a significant alteration in the SMA's response [15, 16]. This makes the characterization of the SMA behavior a challenging task. Descriptions of several experimental apparatuses can be found in the literature, most of which are primarily designed for SMA wires, with only a limited number designed for SMA springs. These experimental systems are usually composed of mechanical and thermal units that operate simultaneously. The mechanical unit provides the means for controlling and measuring the specimen elongation and applied force and the thermal unit provides the means for controlling its temperature.

We formally distinguish between two types of mechanical setups: one in which the applied force is controlled and the deflection is measured, and a second in which the specimen elongation is controlled and the force is measured. In the force-controlled mechanical units, one end of the specimen is attached to a stable frame, while the force is applied at the other end, usually with a hanging weight [14, 17–19]. A resistive displacement transducer [12], an LVDT [20], or a laser sensor [17, 19] is used for measuring the elongation. The displacement-controlled units consist of two parts: the immovable base and the moving part, which we denote as the crosshead. The specimen is connected at one end to the base and at the other to the crosshead. The elongation is controlled by adjusting the crosshead position. The exerted force is measured by a load cell or a force gauge. Industrial motorized testers [13, 21, 22] as well as custom-made systems [16, 23–25] are used. In the industrial testers, the specimen elongation is controlled by a screw-type electromechanical unit and measured by a built-in traveling indicator. In the custom-made testers, the elongation is controlled by a screw-type electromechanical unit [23], a linear motor [16, 24] or a manual mechanism [25], and measured by an LVDT [23], an optical encoder [16, 24] or a camera-based image processing system [25]. One notable advantage of a displacement-controlled apparatus is that it allows for the execution of force-control experiments, wherein a controller continuously adapts the specimen's elongation to uphold the desired force level [16]. For this reason, the displacement-controlled concept was adopted in this work.

Two methods for heating and cooling the specimen are described in the literature. The first is Joule heating in which the specimen is heated by an electric current and cooled down by convection [14, 19]. The temperature is measured directly by thermocouples attached to the specimen [23] or by an infrared camera [17]. Another option is to estimate the temperature from the intensity of the applied electric current based on a-priori collected data [26]. While simple to implement, it is difficult to accurately control the temperature and its rate of change [15].

In the second method, the specimen is placed in an environmental chamber fitted within a mechanical unit [15]. Commonly, the environmental chambers are filled with gas whose temperature is controlled. Resistive heaters are used to heat the chamber [15] and cooling is achieved by air, CO_2, or N_2 flow. The specimen temperature changes through thermal conduction. Industrial environmental chambers were used in [21, 27, 28], and custom-made chambers in [15, 16]. To cope with temperature deviations that can alter the SMA properties, a fan is used to homogenize the temperature inside the chamber [16] or a flow diffuser is attached to the forced-air inlet [15]. The specimen temperature is monitored by an attached thermocouple [22] or by a remote infrared sensor [29]. Environmental chambers are commonly used for constant temperature experiments and only in a few cases transient temperature experiments are feasible (e.g., [30]).

The utilization of liquid as a thermal medium for Nitinol Springs experimental systems is relatively uncommon. However, this practice is widely adopted in various other fields, such as thermal calibration systems. In these systems, a calibrated thermometer and a reference thermometer are positioned in close proximity within a water bath, the temperature of which is meticulously regulated. The uniformity of the environment surrounding the thermometers is upheld by the controlled flow of water in the bath. The temperature range must span between the freezing and the boiling temperatures of the liquid and naturally, water is a suitable choice for biomedical applications. In the context of the present work we recall that a Nitinol experimental system that uses liquid in the chamber is described in [15], based on earlier study [31]. The tested model is immersed in a liquid contained within a bath. The uniformity of the

liquid temperature is maintained with an external temperature-controlled bath circulator. Shaw and Kyriakides [31] measured temperature variations with a few thermocouples set approximately 15mm apart along NiTi wire specimens. They found that in a water bath the variations in the temperature were smaller than 1 °C at a strain rate of 4×10^{-4} s^{-1}. In the present study, where 2% strains are achieved over a span of a few minutes or longer, the strain rates are comparable to or even lower than this. Furthermore, to ensure accurate control of the water temperature and finely tune the cooling and heating rates, a Peltier thermoelectric-based temperature unit is utilized. The thermoelectric Peltier device has two primary advantages. First, the same device heats and cools the water; second, a small quantity of liquid is required, lowering the heat capacity of the system. These enable faster heating and cooling rates and accurate flexible control of the water temperature. To our knowledge, thermoelectric units are rarely used in the context of SMA experimental systems. This results in an acute experimental system that can precisely regulate two of the three state variables while continuously monitoring the third. Additionally, these parameters can be adjusted at any point in time, even during phase transformations. Since the lattice structure of SMA in the martensite phase is history-dependent, experiments with different histories of the sample are expected to produce different results. For this reason, the precise setting of the initial condition of the SMA specimen is crucial, and a few possible options are discussed in the literature. One possibility is to prepare all the specimens from the same material and test each specimen once. In [15], for example, the tested specimens from the same manufacturer spool were used "as received". Another possibility also described in [15], is first to cool the "as received" sample in liquid nitrogen (-196 °C), assuring that the SMA is far below its M_f temperature, and then heat it to the required experimental temperature. A third possibility, appropriate in cases where the same specimen is repeatedly tested, is to heat the unloaded specimen to a temperature above A_f before every experiment. Thus, the SMA is fully in the austenite phase prior to the experiment and its lattice structure is unambiguously defined [12]. Herein, as we utilized the same Nitinol spring specimen for a series of experiments, we opted for the third method. To guarantee uniform initial conditions for all samples and ensure the consistency of measurements, we devised an innovative calibration procedure that entails subjecting the spring to a cooling and heating cycle while it is load-free. This procedure was made possible due to the ability to accurately control and monitor the temperature.

The remainder of this article is arranged as follows: Sect. 2 describes the experimental system and its operation. The experimental setup, including the preparation of the Nitinol spring samples and the calibration procedure are discussed in Sect. 3. The results of representative experiments are depicted in Sect. 4 and finally, in Sect. 5, the main achievements are summarized.

Experimental System

We designed and constructed an experimental apparatus that enables controlling and measuring the three parameters that govern the SMA spring state: temperature, elongation, and force. The apparatus is aimed at meeting generic requirements for bio-medical devices, where commonly large elongations and relatively small forces are needed. A sketch of the experimental system is shown in Fig. 1. The system comprises four main components: the bath, the thermal unit, the mechanical unit, and the control. On the right side, the entire system is sketched, and on the left side, the sketch of the bath is enlarged. A photo of the bath is shown in Fig. 2 with a Nitinol spring specimen. The spring is connected to the bath base at one end and the force gauge at its other end.

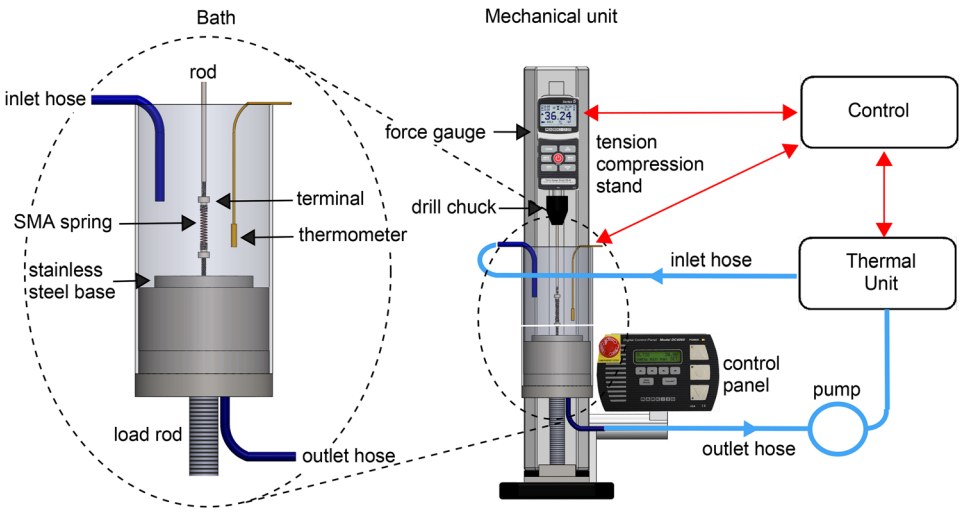

Fig. 1 The experimental system. Right: the entire apparatus. Left: The bath (enlarged)

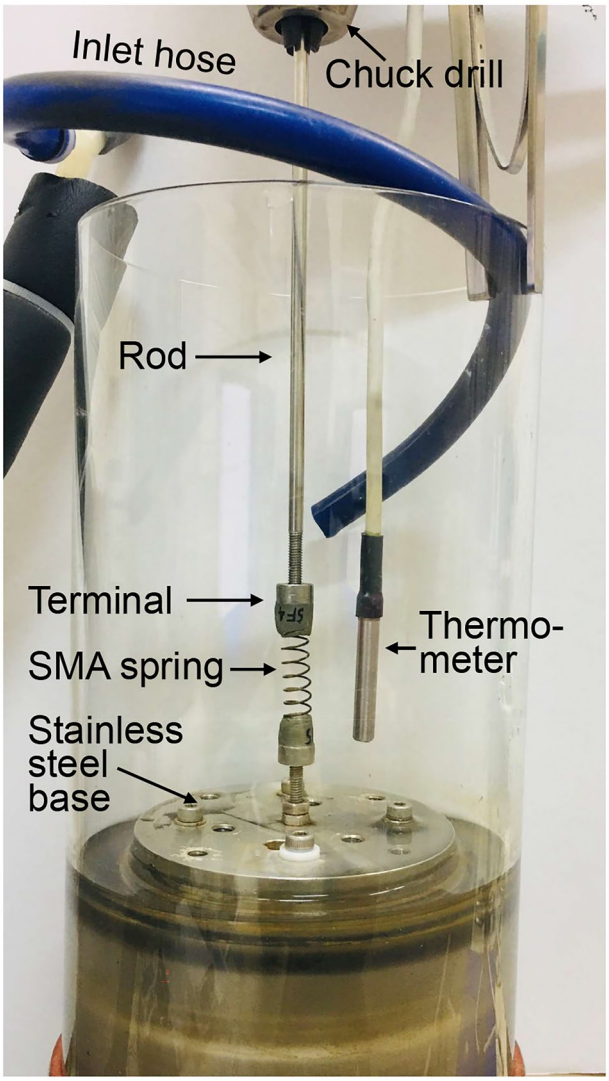

Fig. 2 Photo of the bath with an SMA spring before it is filled with water

When the bath is filled with water, the spring is completely immersed. This setting allows for controlling the temperature of the spring by controlling the water temperature. Together with the spring a PT100 thermometer is also fully immersed in the water. The water enters the bath from the silicon inlet hose, whose inner diameter is 6 mm, and exits through the drainage tube at the bottom which is connected to an outlet hose of the same material.

The bath consists of a borosilicate glass cylinder, which is mounted on top of a polycarbonate and stainless steel 316 base. Its transparency enables visual monitoring of the specimen during the experiments. The base is firmly attached to the stand of the mechanical unit by a threaded load rod. The bath inner diameter is 114 mm, and the maximal height of the water pillar is 145 mm. These dimensions allow easy access to the spring assembly with enough space for auxiliary equipment such as the thermometer. To minimize heat losses the bath is partially wrapped by Anavid's Vidoflex® elastomer insulating foam sheet (for clarity, this is not shown in Fig. 2).

TE Technology Inc. CP-200HT-TT thermoelectric Peltier device is the heart of the thermal unit that controls the temperature of the water in the bath. It is powered and controlled by a TE Technology Inc. PS-24-25 power supply and a CT-720 thermoelectric temperature controller respectively. The heating and cooling of the water that flows through are accomplished with two TE Technology Inc. LC-SSX1 heat exchangers that are connected in series. The water is continuously circulated through the heat exchangers and the bath by a Shysky Tech DC50B-12100 S rotary pump. A lever tap manually adjusts the precise flow rate. The Peltier device functions between -25 °C to 100 °C. Due to the design of the thermal unit [32], especially since the water is the thermal conducting medium we use it between 30 °C and 80 °C, where the heating/cooling power is adequate for a heating/cooling rate of approximately 2 °C/min. The heated/cooled water circulates through the inlet hose into the bath and then through the outlet hose and the pump to the heat exchanger unit and back to the inlet hose. To minimize heat losses the heat exchangers and the hoses are wrapped by Anavid Vidoflex® elastomer insulating foam sheets and tubes. For monitoring the system during the experiment the temperatures of the cold plate of the Peltier unit and the pump are measured by two thermistor thermometers.

We meticulously regulate the flow of water to guarantee thermal uniformity inside the bath. The water circulates through the TE Peltier device and the bath at a flow rate of up to 3.4 liters per minute, resulting in 2-3 complete replacements of the bath water (1.0−1.5 liters) every minute. A quasi-static condition is achieved by controlling the rate of temperature change, ensuring it is 2 °C per minute or less. Overall, the temperature control accuracy is ±0.5 °C. We recall that the mass of the water is much larger than that of the specimen, and because both its spatial and temporal temperature variations are small, we assume that the water temperature measured by the thermometer in the vicinity of the spring is identical to the spring temperature. Moreover, as the Nitinol is a conductor, under these uniform conditions its temperature is almost uniform [31].

The mechanical unit is composed of a tension-compression MARK-10 ESM303 1.5kN motorized stand and an integrated MARK-10 M5-5 25N force gauge. The tested spring ("SMA spring" in Fig. 1) is connected between the bath base, which is firmly connected to the stand base and a drill chuck through a connecting rod. The chuck, which is used as a gripper, is connected to the force gauge that is attached to the moving crosshead of the stand (the crosshead is not shown in Fig. 1). By raising or lowering the crosshead the spring is tensed or compressed. The applied force

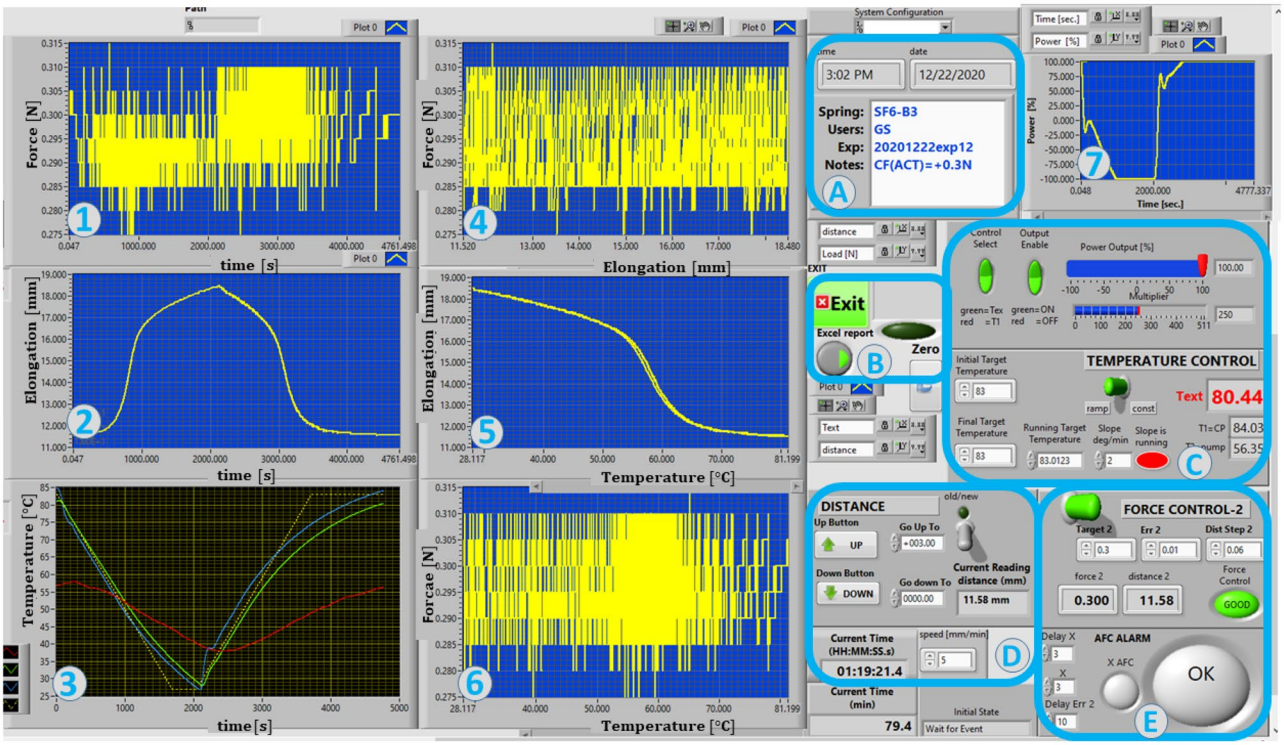

Fig. 3 A snapshot of the LabVIEW GUI (Exp. GS-12a)

is measured by the force gauge with a resolution of 0.005N and a full capacity of ±25N (tension or compression). The force is measured relative to a zero force state set by pressing the "zero" key in the force gauge control panel. The position of the crosshead is measured by a built-in *encoder* with a resolution of 0.02mm and a maximum travel distance of 457 mm. The crosshead parameters, such as its position, upper and lower limits, and speed, are controlled by and displayed on the MARK-10 ESM303's built-in *Control Panel*. Similarly, the M5-5 force gauge parameters are displayed on and controlled by its panel.

The experimental system is controlled by a dedicated PC running a NI LabVIEW software (revisions 2018a and 2020a) which also displays the measured parameters on the computer monitor. The communication with the MARK-10 ESM303 stand and the TE TC-720 controller is accomplished via USB interfaces. The thermometer reading is acquired via a National Instruments NI PCI-6251 data acquisition card. In the course of the experiments the spring temperature, its elongation, and the applied force are sampled approximately every 0.3 s by a self-coded LabVIEW program. During the experiments, a front panel is displayed on the computer monitor that serves as a Graphical User Interface

Table 1 The GUI graphs

	Monitored Variable(s)	Vertical Axis	Horizontal Axis
1	Force vs. Time	[N]	[s]
2	Elongation vs. Time	[mm]	[s]
3	Temperature vs. Time		
	Bath temperature - green		
	Required (target) temperature - dashed white	[°C]	[s]
	Cold plate temperature - blue		
	Pump temperature - red		
4	Force vs. Elongation	[N]	[mm]
5	Elongation vs. Temperature	[mm]	[°C]
6	Force vs. Temperature	[N]	[°C]
7	The ratio of the Peltier device power to its positive maximum value vs. Time	[%]	[s]

Table 2 Tested Nitinol spring specimen dimensions

Spring	SF1a2	SF2	SF2a	SF3	SF4	SF5	SF6	SF7
No. of active coils []	8.0	9.0	8.0	8.5	5.5	6.0	9.5	12.0

(GUI). Upon completion of the experiment, the sampled data is saved to an Excel file for further processing. A snapshot of the front panel is also saved as a concise visual record of the experimental data. In Fig. 3 the LabVIEW GUI is shown at the end of a representative experiment. Numbers mark the seven graphs whose descriptions are detailed in Table 1. The five primary control panels are framed and marked by letters. For conciseness, in Appendix A we describe the various control algorithms.

Experimental Setup

Eight Nitinol spring specimens were prepared from SAES Getters SmartFlex® tensile springs, Manufacturer code 5S8004, with typical A_s between 50 °C and 55 °C and maximal tensile force at the martensitic phase of 2.0N. They were delivered as "trained" and no significant performance difference was detected in successive experiments. Aside from the number of coils their geometrical parameters are identical. The wire diameter is 0.63mm, the coil mean diameter is 6.63mm and the spring index is 10.5. The number of coils in each sample is listed in Table 2.

Shown in Fig. 4(a) and (b) are the spring (as supplied) and the terminals, respectively. Shown in Fig. 4(c) are the two stages of the spring assembly procedure. Initially, the spring hooks were removed and a spring section with the required number of coils was cut off. A typical spring specimen contains 6 to 12 active coils with 3 to 5 extra coils at each end. The extra coils are screwed onto the M7 thread of the stainless steel terminals (top of Fig. 4(c)) and then adhered to the terminals with Hercules Propoxy® glue (bottom of Fig. 4(c)). To remove undesired residues the spring and the terminals were dipped in an alcohol solution prior to adhesion. The two M4 inner threads of the terminals are used for connecting the spring assembly to the experimental system.

We estimate the total weight of the moving parts to be

$$W_A = \frac{W'_N}{2} + W_R \tag{1}$$

where W_R is the weight of the connecting rod and W'_N is the weight of the Nitinol spring specimen when it is immersed in water. The weight of the spring specimen is divided by 2 as an approximation since its lower end is attached to the bath base. During the experiments, the portion of the connecting rod immersed in the water depends on the temporal elongation of the specimen. The variation in the length of the immersed section Δh affects the value of W_A due to the Archimedes effect. Thus, the variation in W_A is:

$$\Delta W_A = S \cdot \Delta h \cdot \rho_W \tag{2}$$

where ρ_W is the specific weight of the water and S is the rod cross-section. The diameter of the connecting rod is 4 mm. Since in most of the experiments $\Delta h < 20$mm the variations in W_A are smaller than 2.5mN. This is smaller than the resolution of the force gauge and has a minor effect on the measured results. The weight W_A is required for the calibration procedure that is described next.

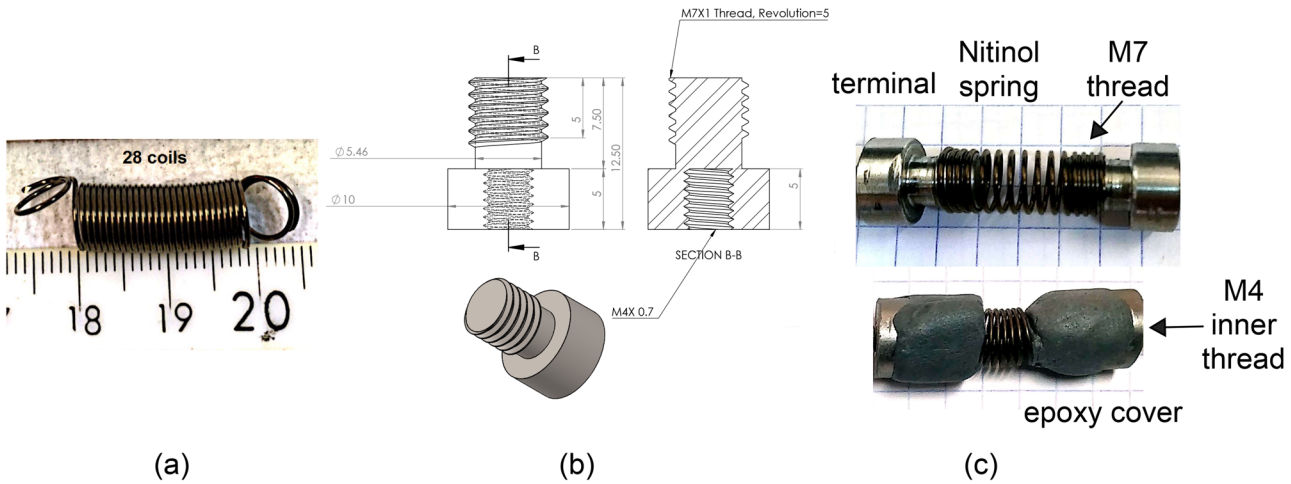

Fig. 4 The assembly process of a Nitinol spring specimen, (**a**). the spring as supplied, (**b**). a drawing of a terminal, (**c**). the spring is threaded onto the terminals and finally glued

The purpose of the calibration procedure is to establish the load-free state of the Nitinol spring before performing any experiment. This step is crucial to guarantee the consistency and repeatability of the measurements. Initially, while the bath is empty, the force gauge is zeroed while the drill chuck hangs freely from the lower thread of the force gauge. Next, the lower terminal of the spring specimen is screwed to the M4 thread at the bath base and the connecting rod is screwed to its upper terminal (see Fig. 2). Finally, the rod is firmly connected to the drill chuck. Once the specimen is in place, the bath is filled with water, ensuring that the spring and the thermometer are entirely immersed. Since a unique load-free state of the Nitinol is defined only in the austenite phase, we initiate the calibration procedure at a temperature of 80 °C, which is above A_f. Thus, the water is heated to 80 °C and the crosshead is elevated to a position where the applied force reading is equal to W_A. This indicates that the net force acting on the spring is zero since the total force is equal to the weight of the moving parts of the spring assembly. At this position, both, the force gauge and the traveling display are zeroed, fixing the reference load-free state of the spring.

Next, to validate that this is indeed the free state, a temperature cycle from 80 °C to 30 °C and back to 80 °C is completed while the length of the spring is held fixed. This temperature range covers the one used in our experiments. If the fluctuation of the force during this cycle is smaller than a threshold of 0.05N, the calibration procedure is completed. Otherwise, the crosshead free state position is slightly changed, and the cooling heating cycle is repeated till the variations in the force are smaller than the threshold. The threshold value of 0.05N was chosen as it is an order of magnitude smaller than the typical loads applied on the spring and an order of magnitude larger than the resolution of the force gauge. The results of a typical calibration procedure are shown in Fig. 5, where the measured temporal variations of the bath temperature (orange) and the measured force (blue) are presented. The spring is cooled to 30 °C and heated back to 80 °C while the spring ends are firmly held and the force is monitored.

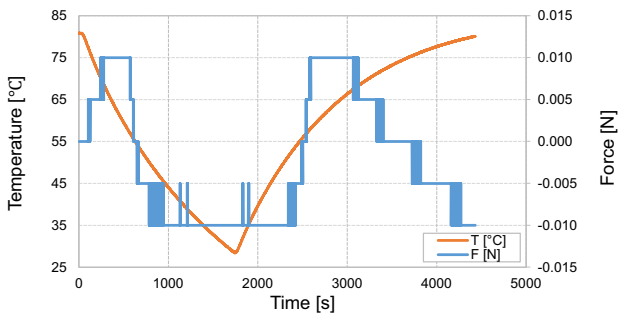

Fig. 5 Temporal variations of the temperature and the force during calibration of SF6 in experiment GS-15

The maximal force of +10mN is attained between 70 °C and 57 °C during both cooling and heating. The force is reduced to -10mN between 57 °C and 30 °C. The total fluctuation in this typical calibration was 0.020N, which is accepted as a successful calibration. Note that the ability to continually control and monitor the temperature is essential for carrying out the calibration process.

Experimental Procedures and Results

Throughout, each experiment is given a unique title, and a list of the experiments with their main parameters is presented in Table 4 of Appendix B. *Constant Elongation* (CE) experiments are ones in which the specimen elongation is prescribed and the force required to maintain it is measured while the temperature varies. Initially, at a temperature above A_f (about 80 °C), the crosshead is moved to the position where the prescribed elongation is attained. It is maintained in this position until the end of the experiment. In a common CE experiment, the temperature is decreased until a target temperature below M_f (about 30 °C) is attained and the cycle is completed when the temperature is raised back to the one above A_f. The force that the spring extracts on the crosshead is monitored and recorded during the entire CE procedure.

In Fig. 6 the responses of spring SF3 during two CE experiments (Exp. ES-6) are depicted. Shown in Fig. 6(a) are the temporal variations of the controlled temperature (dashed lines) and measured force (solid lines) at constant elongations of 6 mm (blue) and 15 mm (orange). Shown in Fig. 6(b) are the variations of the forces versus the temperature that were extracted from the measurements during these two experiments. The 6 mm CE experiment began at 80 °C, where the measured force was at its maximal value of 1.08N. Then, the spring was cooled to 30 °C, assuring that the Nitinol was in the martensite phase, where the force decreased to its minimal value of 0.335N. The reduction in the force is primarily due to the detwinning of the material as it transforms from austenite to martensite. This can be seen in the forces versus temperature curves, where in the intermediate temperature range (50 °C to 65 °C) there is a transition zone in which the force rapidly decreases. The lower modulus of the material in the martensite phase also contributes to the reduction in the forces.

Once the lowest temperature was reached the spring was heated back to 80 °C and the force increased to its initial value. The force versus temperature curve, shown in Fig. 6(b), is characterized by three distinctive sections. At high (above 65 °C) and low (below 50 °C) temperatures, the slopes of the curve are rather small. In the intermediate range (50 °C to 65 °C) there is a transition zone where the force rapidly increases. This is the “shape memory” effect

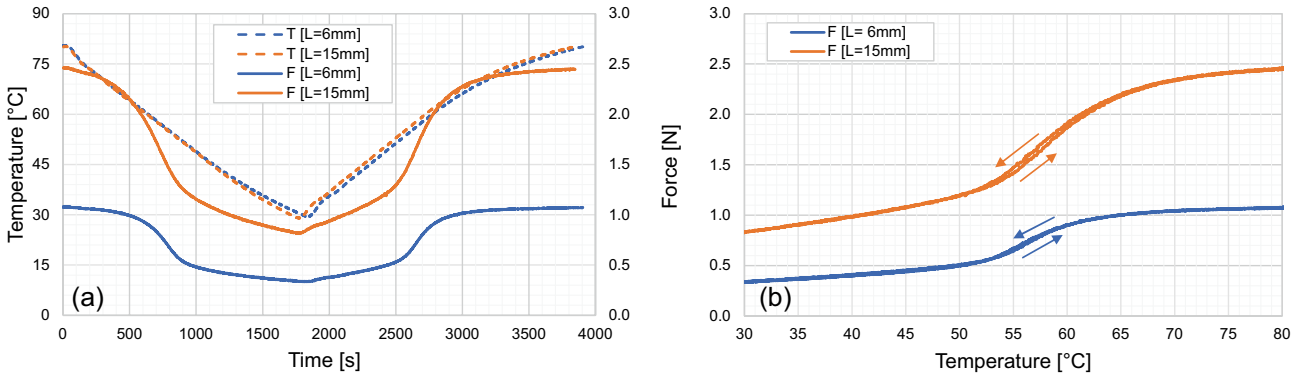

Fig. 6 Constant Elongation experiments with spring SF3 at L=6 mm and 15 mm. (**a**) variations of the temperature (left axis) and the force (right axis) versus time. (**b**) variations of the force versus the temperature

during which the detwinned martensite transforms back to austenite. The anticipated hysteresis in the transition zone manifests as a small difference between the forces during the cooling and heating stages, with the force during the cooling stage being slightly higher. A similar response is observed during the 15 mm CE experiment, where the maximal force is 2.46N and the minimal force is 0.82N.

Constant Force (CF) experiment is one in which the temperature is altered and the elongation is measured while a prescribed force is kept fixed. To this end, the closed-loop control procedure described in Appendix A was implemented. Typical increments of the crosshead location are 0.06mm and the corresponding force variations are 20mN. The behavior of spring SF4 in CF experiments (Exp. ES-10) is demonstrated in Fig. 7. Shown in Fig. 7(a) are the temporal variations of the controlled temperature (dashed lines) and the resulted elongations with constant forces of 0.94N (continuous blue curves) and 2.0N (continuous orange curves). Shown in Fig. 7(b) are the variations of the resulted elongations versus the temperature in these two experiments. The 0.94N constant force experiment began at 80 °C where the elongation was 3.36mm. The spring was then cooled to 30 °C and elongated to its maximal value of 10.18mm. Once the lowest temperature was reached the spring was heated back to 80 °C and the spring elongation decreased to 3.4mm, close to the initial state. The 2.0N CF experiment was executed in a broader temperature range between 80 °C and 20 °C. Due to the larger applied force, the elongations at 80 °C and at 20 °C were 7.22 and 32.84mm, respectively. The hysteresis in this cycle is substantially larger than the one observed during the 0.94N cycle. The results of these experiments are essentially reciprocals of the constant elongation experiments. Thus, the elongation of the springs along the cooling stage is due to the martensite detweening during the phase transition. This occurred within a small temperature range as can be seen in the elongation versus temperature plots. Upon heating the spring shortens as the detweened martensite transforms back to austenite.

Isothermal - Constant Temperature (CT) experiment is one during which the specimen is held at a prescribed constant temperature. The procedure is initialized at a temperature above A_f (about 80 °C) when the spring is adjusted to

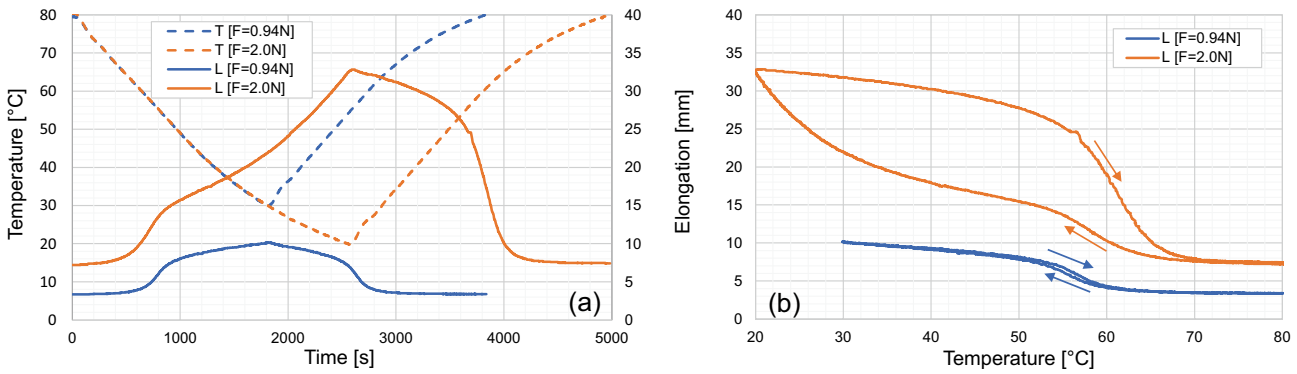

Fig. 7 Constant force experiment at F=0.94N and 2.0N of spring SF4. (**a**) variations of the temperature (left axis) and the elongation (right axis) vs. time. (**b**) variations of the elongation vs. temperature

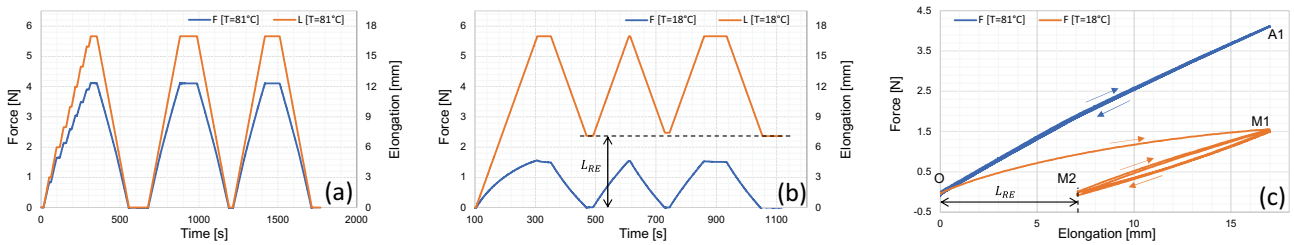

Fig. 8 Isothermal experiments IA-1910. (**a**) and (**b**) The force and elongation versus time at 81 °C and 18 °C, respectively. (**c**) The force versus the elongation curves at the two temperatures

its load-free state. Next, the temperature is varied until the prescribed temperature is achieved. At this temperature, the elongation (force) is imposed and the force (elongation) is measured and recorded. Usually, the procedure is repeated three to four times. The behavior of spring SF4 in CT experiments IA-1910 is demonstrated in Fig. 8. Shown in Fig. 8(a) and (b) are the temporal variations of the spring elongation (orange, right axis) and the applied force (blue, left axis) at 81 °C and 18 °C, respectively. Shown in Fig. 8(c) are the variations of the force versus the elongation at 81 °C (blue) and 18 °C (orange). At both temperatures, the spring was successively stretched and released three times at 5 mm/min.

Note in Fig. 8(a), at 81 °C when the Nitinol is in the austenite phase, the spring was stretched from 0 mm to 16.98mm and returned to its original length upon release. In the process, the force increased to 4.11N and decreased to -0.005N, respectively. To examine the steady-state response of the tensed spring, the stretching stage of the first cycle was intermittently paused eight times for breaks lasting 10 to 15 s each, and at the end of each cycle the spring was held at its maximal elongation of 16 mm for approximately 50 s. It was observed that the force was consistently maintained during these pauses, indicating a consistent spring stiffness overtime at 81 °C when the spring is in the austenite phase.

In Fig. 8(b), at 18 °C when the Nitinol is in its martensite phase, the spring was stretched three times to 16.98mm and then released till the force vanished at a residual elongation (L_{RE}) of approximately 7.1mm. During the first cycle, the maximal elongation of 16.98mm was kept fixed for a period of approximately 50 s. During this time the force decreased from 1.545 N to 1.495 N. A similar slight decrease of the force was observed in successive loading whenever the elongation was held fixed.

Shown in Fig. 8(c) are the measured forces versus the imposed elongations. At 81 °C (blue curve) the spring is stretched from the origin to the maximal elongation and force and, upon release, returned back to its initial state. The three cycles almost coincide with negligible hysteresis. At this temperature, the elastic behavior is almost linear. At 18 °C (orange curve) the spring is stretched from the original state to the maximal elongation and force and then released till the force vanishes at the residual elongation. Note that the spring elongates according to a concave curve during the first cycle. During the second and the third cycles the spring stretched to the maximal length and then shrank back to L_{RE}, with a small hysteresis in the unloading-loading cycles. Thus, in the cold state the spring initially stretched to its maximal length due to a combination of the detwinning process and the elastic deformation. On unloading the elastic deformation decreased and at zero force only the residual elongation of the detwinned martensite remained. During subsequent loading and unloading cycles, the spring stretched elastically to the maximal elongation and shortened back to the residual elongation upon release.

More complicated experiments are ones in which different state variables are controlled during different sections of the experiment. The results of such experiment, GS-13b with spring SF6, are presented in Fig. 9. Curve "a" (blue) presents an experiment in which the spring was cooled at a constant force F=1.2N. At the low temperature, the force was reduced to F=0.9N and the spring was heated back to the initial temperature. Curve "b" (orange) presents the reverse experiment in which the forces during the cooling and heating stages were 0.9 and 1.2N, respectively. We note that the cooling section of curve "a" at constant force F=1.2N and the heating section of curve "b" at the same constant force coincide

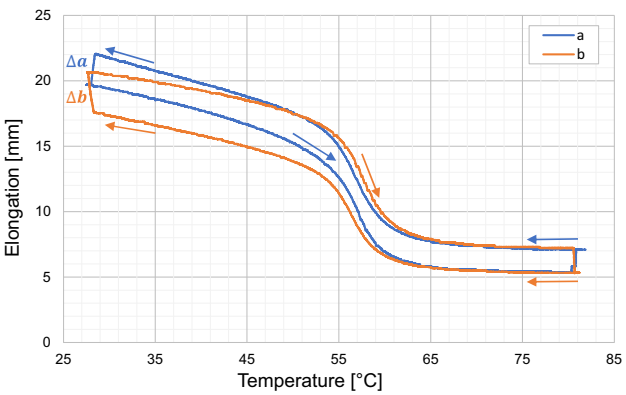

Fig. 9 A circCF experiment GS-13b with spring SF6, (**a**). The spring is cooled at F=1.2N and heated at F=0.9N. (**b**). The spring is cooled at F=0.9N and heated at F=1.2N

Table 3 Data at the instants where the roles of the loading parameters are switched in the experiment shown in Fig. 10

Label	T [°C]	L [mm]	F [N]
A	79.90	3.40	0.700
B	20.30	12.38	0.700
C	28.44	11.86	0.700
D	29.13	9.14	0.340
E	53.35	5.34	0.340
F	20.00	8.38	0.340
G	79.46	1.74	0.350

at temperatures above 57 °C. Similarly, the cooling section of curve "b" and the heating section of curve "a", both at F=0.9N coincide at temperatures above 60 °C. We also note that the displacement Δ_a=2.34mm of the spring along curve "a" when the force decreases from 1.2N to 0.9N is smaller than the displacement Δ_b=2.88mm along curve "b" when the force increases from 0.9N to 1.2N.

The results of another complex experiment (IA-1909-route1) with spring SF1a2 are shown in Fig. 10. The labels in Fig. 10 mark points at which the roles of the loading parameters are modified. The data at these points is listed in Table 3. The experiment is composed of four stages. In the first stage the spring is cooled at a constant force F =0.7N from T_A to T_B and heated back to T_C. In the second stage, the force is decreased from F=0.7N to 0.35N at a constant temperature. In the third stage, the spring is heated to T_E at a constant force F=0.35N. In the fourth stage, the spring is cooled to T_F. Finally, the spring is heated back to T_G at a constant force F=0.35N. We note that section DE, when the spring is heated from T_D to T_E at a constant force, and section EF when the spring is cooled from T_E to T_F at the same constant force do not coincide.

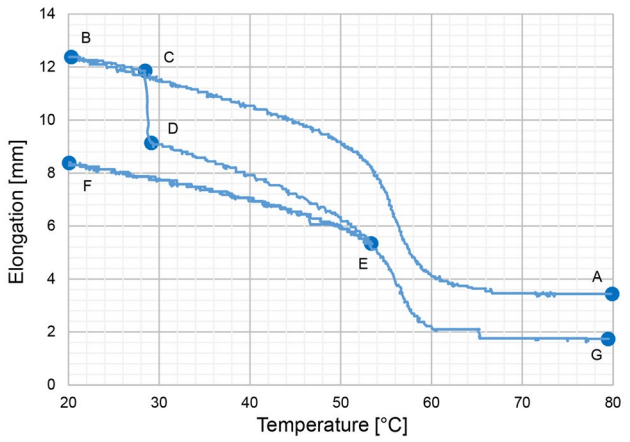

Fig. 10 A complex experiment (IA-1909-route1) with spring SF1a2

Conclusions

We introduce an experimental system for testing and characterizing SMA springs. The system is aimed to fit generic requirements for bio-medical devices, where commonly large elongations and relatively small forces are needed. The system allows accurate control of the three governing state variables: temperature, elongation and force, along with their rates and histories. Specifically, the system enables to control the values and the rates of any two-state variables while monitoring the third. It comprises four main components: the water bath, the thermal unit, the mechanical unit, and the control.

As the temperature control of most reported experimental systems suffers from limited accuracy and rate control capability, herein we adopted a different path. The tested SMA spring is immersed in a water bath that enables precise control of the sample temperature by controlling the water temperature with a thermoelectric Peltier device. We exploit the advantages of this device that can both heat and cool the water while requiring a relatively small amount of water to circulate between the Peltier device heat exchanger and the bath. The water temperature is constantly measured with a thermometer mounted near the sample. The precise temperature control is especially important in the low-temperature martensitic phase.

The mechanical unit comprises a standard tension-compression motorized stand. Its built-in encoder measures the elongation of the spring and the accompanying force gauge monitors the applied force. Force control is achieved by continuously monitoring the measured force and adjusting the spring elongation to maintain the required force. To enable visual monitoring of the spring during the experiment, the bath is made out of a transparent borosilicate glass cylinder mounted on a polycarbonate and stainless steel base. The experimental system control is carried out via the graphic user interface (GUI) of a dedicated LabVIEW program. The GUI presents the temporal dependence of the governing variables along with the control parameters.

To ensure the repetitiveness of the experiments and avoid inaccuracies due to the history dependence of the SMA behavior we found that establishing a methodological calibration procedure is crucial. Initially, the net force on the Nitinol spring is zeroed in its hot phase. This defines a reference point for the elongation, the force and the temperature of the SMA spring at the beginning of each experiment. Next, while fixing the SMA spring length, it is cooled to the low phase and heated again. Throughout this process, it is verified that the variations in the force are smaller than a given threshold. This calibration procedure guarantees that the load-free length of the Nitinol spring is well-defined, thus ensuring consistency of subsequent experimental measurements.

Eight Nitinol springs with 5.5 to 12 active threads were tested under various scenarios. Two typical constant elongation experiments demonstrated the overall response of the Nitinol spring. Beginning at 80 °C, when the spring is in the austenite phase, the maximal forces were measured. Next, while the spring was cooled then, due to the detweinning of the Nitinol, the forces decreased and attained their lowest value at 30 °C when the Nitinol was in the martensite phase. The spring was then heated back to 80 °C and the forces increased to their initial values. Constant force experiments were accomplished with an automated control procedure. The experiments began at 80 °C with minimal elongation of the spring and as the spring was cooled down, it elongated to its full length at 30 °C. The spring was then heated back to 80 °C and shortened to its initial state. As expected, the results of these experiments are essentially the reciprocals of the constant elongation experiments. Two constant temperature experiments, at 18 °C and 81 °C, demonstrated the Nitinol spring responses in its martensite and austenite phases, respectively. At 81 °C the spring exhibited an elastic almost linear behavior. At 18 °C the spring stretched due to a combination of detwinning and the elastic deformation. During subsequent loading and unloading, the spring stretched elastically and shortened to the residual elongation upon release.

The versatility of the experimental system was demonstrated in two complementing experiments during which the controlled state variables were switched. Initially, at the hot phase the spring was stretched and then, at a constant force, cooled to the target low temperature. In the cold state, the force was increased in one experiment and decreased in the other, and then the spring was heated back to the initial temperature. These experiments demonstrated the history dependence of the Nitinol behavior in the martensite phase. Specifically, we show that below the transformation temperature, the response of the spring may be different under similar loading conditions. This was further examined in a third experiment that also involved transitions between constant force and constant temperature segments. Herein, we find that when the force is varied inside the martensite regime, the spring response is different from the one it exhibits in a constant force experiment. Yet, if the spring is heated above the transition temperature and cooled back, the constant force response is recovered.

These experimental results have demonstrated the excellent control capability and flexibility of the system, making it suitable for advancing research on SMA springs and even SMA spring-based actuators. In particular, the system precise temperature control capability provides the means to study the response of SMA springs at the low-temperature phase.

Appendices

A. The GUI and Control Algorithms

Throughout this Appendix, we refer to Fig. 3 where the self-programmed LabVIEW GUI is presented. The temperature of the tested specimen is controlled through panel C. The power of the Peltier device P_{out} **[Power Output [%]]** is varied to maintain the specimen temperature T **[T ext]** as close as possible to the required target temperature T_{tgt} **[Running Target Temperature]**. P_{out} spans from -100% to +100%, which corresponds to full cooling capacity and full heating capacity, respectively. To accomplish this task the bath temperature is sampled with the PT100 thermometer periodically and Pout is adjusted such that

$$P_{out}[\%] = 100 \cdot (T_{tgt} - T) \cdot \frac{(X_{mul})}{512} \tag{3}$$

where X_{mul} **[Multiplier]** is an adjustable parameter. The value $X_{mul} = 250$ was determined by trial and error. In isothermal experiments where the temperature should be constant, T_{tgt} is kept fixed by setting the position of the **[TEMPERATURE CONTROL]** lever to the red **[const]** position. In experiments where a constant rate of temperature change versus time is required, the lever is set to the green **[ramp]** position and T_{tgt} changes at a constant rate **[°C/min]** that is preset in the **[Slope deg/min]** window. Once T_{tgt} reaches the final temperature **[Final Target Temperature]**, it is held constant, and the indicator **[slope is running]** turns from green to red. The performance of the temperature control procedure is demonstrated in the GUI snapshot shown in Fig. 3. Shown in graph 3 are the temporal variations of the temperature. Throughout the experiment, T_{tgt} (white dashed curve) varied from 80 °C to 30 °C and back to 80 °C at -2 °C/min and +2 °C/min, respectively. Note that T (green curve) traces T_{tgt} with an ever-increasing error $T - T_{tgt}$. The temperature versus time rate is limited by the characteristics of the Peltier device [32]. As long as the ambient temperature is fixed during cooling, the performance decreases as the temperature decreases. The opposite happens during heating. Thus, at the beginning of either the cooling or the heating stage, the temperature rate is close to 2 °C per minute and, as the process continues, the rate decreases. The specimen elongation is controlled via the crosshead position in panel D. It moves upwards **[Go Up To]** mm from its current position by pressing the **[UP]** key, and downwards **[Go down To]** mm by pressing the **[DOWN]** key. The crosshead speed is set by the **[speed [mm/min]]** window.

The force exerted by the mechanical unit is controlled through panel E. Force control experiments require a closed-loop control where the crosshead position is varied to maintain the applied force F **[Force 2]** as close as possible to the

required target force F_{tgt} **[Target 2]**. To accomplish this task the force gauge is sampled periodically and the crosshead is shifted by ΔL such that

$$\Delta L = \begin{cases} +\Delta L_{step} & \text{if } (F - F_{tgt}) \le -\Delta F_{err} \\ -\Delta L_{step} & \text{if } (F - F_{tgt}) \ge +\Delta F_{err} \\ 0 & \text{otherwise} \end{cases} \quad (4)$$

where ΔF_{err} **[Err 2]** is the tolerance about the target force and ΔL_{step} **[Dist Step 2]** is the discrete step by which the crosshead is shifted. The values ΔF_{err}=0.01N and ΔL_{step}=0.06mm were determined by trial and error. We note that the chosen ΔF_{err} is twice the resolution of the force gauge and ΔL_{step} is three times the resolution of the MARK-10 built-in encoder. The performance of the force control procedure is demonstrated in the GUI snapshot shown in Fig. 3 where the target force **[Force 2]** is F=0.3N. Note in the graph showing the temporal variations of the force (graph 1) that throughout the experiment the applied force varied between 0.285 and 0.310N. These variations are rather small and close to the resolution of the force gauge. The experiment terminates when the green button **[Exit]** in panel B is "pressed". It turns red, and the acquired data is saved to an Excel file.

Faults in the communication between the LabVIEW program and the MARK 10 stand during the experiments cause the force control to halt. If no immediate action is taken, the whole experiment is lost. To avoid this situation, an alarm procedure was implemented to warn the user. In either one of the two scenarios the alarm goes off:

1. ΔF is larger than x **[X]** times ΔF_{err} for a time period longer than t_{del} **[Delay X]**.
2. ΔF is larger than ΔF_{err} for a time period longer than t_{del2} **[Delay Err 2]**.

In addition, the **[X ACF]** control turns red when the first scenario is true, while the **[OK]** control turns red and the caption is changed to **[AFC Alarm]** when the second scenario is true. The alarm parameters t_{del}=3 s, x=3, t_{del2} =10 s, were defined by a trial and error.

B. A List of the Experiments

Table 4 The experiments' main parameters and the corresponding data files

ExpNo.	Spring	Type	Main Parameters	Excel File(s)	Fig.
ES-6	SF3	CE	L=6, 15 mm, T=80 °C - 30 °C	40_ Elongation.xlsx 100_Elongation.xlsx	6
ES-10	SF4	CF	F=0.94, 2.0N, T=80 °C - 30 °C	75_ Force.xlsx 2 N Force.xlsx	7
GS-12	SF6-B3	ACF	F=+0.3N, X0=10.5mm	20201222exp12-CF(ACT)-(3N).xlsx	3
GS-13	SF6	circCF	F=0.9-1.2N, 1.2N-0.9N	20210105exp13-circles-b−1.2−0.9.xlsx 20210105exp13-circles-b−0.9−1.2.xlsx	9
GS-15	SF6	CT	T=80 °C	20210310exp15-calibration.xlsx	5
IA-1909	SF1a2	comp	F=0.70N,T=80,20, 30 °C F=0.35N,T=30,53,20,80 °C	SF1a2-2019-06-03-Route_1-(0.70N)-80,20,(0.35N),53,20,80.xlsx	10
IA-1910	SF4	CT	T=81 °C, Lmax=17 mm, Fmax=4.11N T=18 °C, Lmax=17 mm, Fmax=1.510N LRE=7.10mm	Exp.1_1 SF4 20190822.xlsx Exp.1_3 SF4 20190822.xlsx	8

Acknowledgements We would like to acknowledge Dr. Israel Bronstein and his technical team for their invaluable assistance in constructing the system, Dr. Yeshayahu Weiss for his contributions to the understanding of the heat exchange system, Shai Sharabi for his guidance and support in developing the LABVIEW-based control algorithm, and Ilia Zilberman for his role in initiating the system design and continued input of ideas. The senior-year students who participated in the construction of the experimental system, carried out some of the experiments, and shared their ideas as part of their senior year projects: Sariel (Shira) Sror and Eva Golan, Shani Davidian and Jessica Melman, Or Antebi and Alon Ben Shoshan, Gili Hachmon and Sagi Dadosh of Ben Gurion University of the Negev, and Eli Setzer, a student intern from the University of Arizona. Special thanks to Dr. Doron Goldberg of Tel-Hai College, Israel, who enriched us with his ideas.

Funding Open access funding provided by Ben-Gurion University. Open access funding provided by Ben-Gurion University.

Data Availability Raw images and data generated during the current study are available from the corresponding author upon reasonable request.

Declarations

Conflict of Interest The authors declare that they have no known competing financial interests or personal relationships that could have appeared to influence the work reported in this paper.

References

1. Ryhänen J (1999) Biocompatibility evaluation of nickel-titanium shape memory metal alloy. Oulun yliopisto
2. Bhattacharya K (2003) Microstructure of Martesite: why it forms and how it gives rise to the shape-memory effect, 1st edn. Oxford University Press
3. Lagoudas DC (2008) Shape memory alloys: modeling and engineering applications. Springer
4. ASTM (2010) F2005 standard terminology for nickel-titanium shape memory alloys. Annual Book of ASTM Standards 05:16–18
5. Nespoli A, Besseghini S, Pittaccio S, Villa E, Viscuso S (2010) The high potential of shape memory alloys in developing miniature mechanical devices: A review on shape memory alloy miniactuators. Sens Actuators A 158:149–160
6. Machado L, Savi M (2003) Medical applications of shape memory alloys. Braz J Med Biol Res 36:683–691
7. Sun L, Huang W, Ding Z, Zhao Y, Wang C, Purnawali H, Tang C (2012) Stimulus-responsive shape memory materials: A review. Mater Des 33:577–640
8. Elahinia MH (2016) Shape memory alloy actuators: design, fabrication, and experimental evaluation. John Wiley & Sons
9. Jani JM, Leary M, Subic A, Gibson MA (2014) A review of shape memory alloy research, applications and opportunities. Mater Des 56:1078–1113
10. Otsuka K, Wayman C eds. (1999) Shape memory materials. Cambridge University Press
11. Aguiar RAAD, Pereira JHI, Souza CGD, Pacheco PMCL, Savi MA (2009) Shape memory alloy helical springs : modeling, simulation and experimental analysis. In Mechanics of Solids in Brazil, pp. 169–181
12. Aguiar RAA, Savi MA, Pacheco PMCL (2010) Experimental and numerical investigations of shape memory alloy helical springs. Smart Mater Struct 19:25008
13. An SM, Ryu J, Cho M, Cho KJ (2012) Engineering design framework for a shape memory alloy coil spring actuator using a static two-state model. Smart Mater Struct 21:16
14. Yates S, Kalamkarov A (2013) Experimental study of helical shape memory alloy actuators: Effects of design and operating parameters on thermal transients and stroke. Metals 3:123–149
15. Churchill CB, Shaw JA, Iadicola MA (2009) Tips and tricks for characterizing shape memory alloy wire: Part 2 - fundamental isothermal responses. Exp Tech 33:51–62
16. Auricchio F, Scalet G, Urbano M (2014) A numerical/experimental study of nitinol actuator springs. J Mater Eng Perform 23:2420–2428
17. Aguiar R, Neto WL, Savi MA, Pacheco P (2013) Shape memory alloy helical springs performance: Modeling and experimental analysis. Mater Sci Forum 758:147–156
18. Mammano GS, Dragoni E (2014) Functional fatigue of ni-ti shape memory wires under various loading conditions. Int J Fatigue 69:71–83
19. Grossmann C, Frenzel J, Sampath V, Depka T, Oppenkowski A, Somsen C, Neuking K, Theisen W, Eggeler G (2008) Processing and property assessment of niti and niticu shape memory actuator springs. Materialwissenschaft und Werkstofftechnik: Entwicklung, Fertigung, Prüfung, Eigenschaften und Anwendungen technischer Werkstoffe 39:499–510
20. Elahinia MH, Ahmadian M (2005) An enhanced sma phenomenological model: I. the shortcomings of the existing models. Smart Mater Struct 14:1297
21. Kim SW, Lee JG, An S, Cho M, Cho KJ (2015) A large-stroke shape memory alloy spring actuator using double-coil configuration. Smart Mater Struct 24:095014
22. Rao A, Srinivasa AR (2013) A two species thermodynamic preisach model for the torsional response of shape memory alloy wires and springs under superelastic conditions. Int J Solids Struct 50:887–898
23. Lee HJ, Lee JJ (2000) Evaluation of the characteristics of a shape memory alloy spring actuator. Smart Mater Struct 9:817–823
24. Cadelli A, Manjeri R, Sczerzenie F, Coda A (2016) Uniaxial prestrain and free recovery (upfr) as a flexible technique for nitinol characterization. Shape Memory and Superelasticity 2:86–94
25. Chairez I, Cortez-Vega R, Luviano-Juárez A, Feliu-Batlle V (2018) A hybrid dynamic model of shape memory alloy spring actuators. Measurement 114:340–353
26. Follador M, Cianchetti M, Arienti A, Laschi C (2012) A general method for the design and fabrication of shape memory alloy active spring actuators. Smart Mater Struct 21:115029
27. Deberg L, Andani MT, Hosseinipour M, Elahinia M (2014) An sma passive ankle foot orthosis: Design, modeling, and experimental evaluation. Smart Mater Res 2014:572094
28. Chapman C, Eshghinejad A, Elahinia M (2011) Torsional behavior of niti wires and tubes: Modeling and experimentation. J Intell Mater Syst Struct 22:1239–1248

29. Urbano M, Coda A, Giannantonio R (2006) Smaq: A novel integrated instrument for the characterization of sma wires. In Proceedings of the International Conference on Shape Memory and Superelastic Technologies (SMST 2006), pp. 177–184
30. Gédouin PA, Pino L, Chirani SA, Calloch S, Delaleau E, Bourgeot JM (2019) R-phase shape memory alloy helical spring based actuators: Modeling and experiments. Sensors Actuators A Phys 289
31. Shaw JA, Kyriakides S (1995) Thermomechanical aspects of niti. J Mech Phys Solids 43:1243–1281
32. TE Technology Inc. (2018) CP-200HT-TT peltier-thermoelectric cold plate cooler